Eur Biophys J (2011) 40:1061–1069
DOI 10.1007/s00249-011-0722-3

ORIGINAL PAPER

A fast and robust method for automated analysis of axonal transport

Oliver Welzel · Jutta Knörr · Armin M. Stroebel · Johannes Kornhuber · Teja W. Groemer

Received: 21 January 2011 / Revised: 8 April 2011 / Accepted: 2 June 2011 / Published online: 22 June 2011

Abstract Cargo movement along axons and dendrites is indispensable for the survival and maintenance of neuronal networks. Key parameters of this transport such as particle velocities and pausing times are often studied using kymograph construction, which converts the transport along a line of interest from a time-lapse movie into a position versus time image. Here we present a method for the automatic analysis of such kymographs based on the Hough transform, which is a robust and fast technique to extract lines from images. The applicability of the method was tested on simulated kymograph images and real data from axonal transport of synaptophysin and tetanus toxin as well as the velocity analysis of synaptic vesicle sharing between adjacent synapses in hippocampal neurons. Efficiency analysis revealed that the algorithm is able to detect a wide range of velocities and can be used at low signal-to-noise ratios. The present work enables the quantification of axonal transport parameters with high throughput with no a priori assumptions and minimal human intervention.

O. Welzel and J. Knörr contributed equally to this work.

Electronic supplementary material The online version of this article (doi:10.1007/s00249-011-0722-3) contains supplementary material, which is available to authorized users.

O. Welzel (✉) · A. M. Stroebel · J. Kornhuber · T. W. Groemer
Department of Psychiatry and Psychotherapy, Friedrich-Alexander University of Erlangen-Nuremberg, Schwabachanlage 6, 91054 Erlangen, Germany
e-mail: oliver.welzel@uk-erlangen.de

J. Knörr
Department of Obstetrics and Gynaecology, Sozialstiftung Bamberg, Buger Straße 80, 96049 Bamberg, Germany

Keywords Hough transform · Hippocampal neurons · Axonal transport · Fluorescence microscopy · Kymograph · Vesicle sharing

Introduction

Cargo transport along nerve processes is indispensable for neuronal differentiation and survival, and therefore plays an important role for the whole neural network (Salinas et al. 2008). Synapses require material from the neuronal soma, and thus synaptic transmission depends on axonal transport (Shakiryanova et al. 2006). Furthermore, neurodegenerative diseases are connected to deficits in axonal transport and are thought to represent a critical component in their pathogenesis (Morfini et al. 2009; Roy et al. 2005). Axonal transport is impaired in Huntington's disease (Roze et al. 2010) and in amyotrophic lateral sclerosis (Bilsland et al. 2010). Furthermore, several pathogens such as viruses and toxins can be mistaken for cargo and undergo axonal transport to the soma (Salinas et al. 2010). Axonal transport is often analyzed using wide-field fluorescence microscopy to visualize specific fluorescently labeled cargoes (Miller and Sheetz 2004; Roy et al. 2007). In contrast to former methods such as radioactive labeling (Ekstrom and Kanje 1984), it has the advantages of high spatial (about 200 nm) and time (less than 1 s) resolution. Besides manual tracking (Miller and Sheetz 2004; Roy et al. 2007), mainly two automated methods have been established (1) the particle tracking in time-lapse movies (Sbalzarini and Koumoutsakos 2005; Smal et al. 2008) and (2) the analysis of kymograph images (Welzel et al. 2010; Zhang et al. 2011). Creating a kymograph means converting a time-lapse movie along a line of interest into a position versus time image (Zhang et al. 2011; Zhou et al. 2001). Particles

moving along this line of interest appear as trajectories with their slope corresponding to their velocity. The advantage of kymograph images is the data reduction (Zhang et al. 2011) and graphical representation of particle movements in a single image (Miller and Sheetz 2004, 2006). Furthermore the signal-to-noise ratio can be increased because of averaging or taking the maximum of some pixels around the drawn line of interest. The main disadvantage of a kymograph is the inevitable information loss due to data compression (Pereira and Maiato 2010). As one component of the velocity $\vec{v}$ is lost because drawing a line of interest, the velocity determined in the kymograph image will be an underestimate of the velocity $\vec{v}$ (Pereira and Maiato 2010). However, the error has been reported to be limited to less than 3% if the particle moves nearly along a line (Pereira and Maiato 2010). The manually drawn line of interest could differ from the real particle movement and increase the error in velocity determination. Analysis of transport using kymographs is used for many different research interests in fluorescence microscopy, e.g., neuronal protein traffic (Roy et al. 2007), mitosis and meioses (Pereira and Maiato 2010), axonal transport of mitochondria (Miller and Sheetz 2006) and microtubule dynamics (DeBolt et al. 2007). The analysis of kymographs is mostly done manually by tracing moving particles (Roy et al. 2007) or determining the slopes of trajectories in kymograph images (Miller and Sheetz 2004). Recent studies presented algorithms for the automated analysis of kymographs using auto- and cross-correlation of kymograph columns (Welzel et al. 2009) or the tracking of individual trajectories (Zhang et al. 2011). However, these methods require relatively high signal-to-noise ratios as they only take into account the local area (Zhang et al. 2011) or two kymograph columns (Welzel et al. 2009). Furthermore, the velocity determination is abstracted to cross-correlation (Welzel et al. 2009), or some a priori mathematical modeling of the motion is used (Zhang et al. 2011), which handicaps their usage and implementation.

Here we made use of the Hough transform (Hough 1962), which is a robust and fast method to extract lines in image analysis (Kamat and Ganesan 1995). This algorithm has been successfully applied to line detection in several disciplines such as the automotive industry (Kamat and Ganesan 1995; Yanamura et al. 2003; Yu and Jain 1997) and computer vision (Ballard 1981) because of its robustness and processing speed. Furthermore, the automated detection of lines resembles the hand-drawn traces of movements (Miller and Sheetz 2004; Zhou et al. 2001) and thus realizes their slope similarly to the human eye.

For direct comparison with recent studies, we analyzed axonal transport of synaptophysin (Roy et al. 2007) and tetanus toxin (Lalli et al. 2003). Synaptophysin is a ubiquitous presynaptic marker and is related to the slow component-b (Roy et al. 2007). Further, it is transported anterograde and retrograde with about 1 μm/s (Roy et al. 2007). It has been shown that synaptophysin interacts with VAMP2 (vesicle-associated membrane protein 2) and alters its default surface targeting to a prominent vesicular distribution (Bonanomi et al. 2007). Therefore, it plays an important role in the exocytic pathway of other synaptic vesicle proteins. Tetanus toxin, the causative agent for tetanus, is sorted to the retrograde transport pathway after internalization (Deinhardt et al. 2006; Lalli et al. 2003). Tetanus toxin as well as its heavy chain C-terminal fragment is transported in retrograde carriers with identical kinetic properties and an average velocity of about 1 μm/s (Bohnert and Schiavo 2005; Lalli et al. 2003). Furthermore, we determined the velocity of synaptic vesicles in the vesicle superpool (Darcy et al. 2006; Staras et al. 2010). Here recycling synaptic vesicles are shared between synaptic terminals (Darcy et al. 2006). These superpool vesicles are highly mobile, can be rapidly exchanged and be exocytosed in adjacent terminals upon stimulation (Darcy et al. 2006; Staras et al. 2010). Using the Hough transform for velocity determination in kymographs, we for the first time describe the dynamic properties of this synaptic vesicle exchange between terminals.

In summary, we have developed a robust and fast method for the analysis of kymographs based on the Hough transform. The algorithm has been validated on synthetic kymograph images as well as by analyzing particles with known velocities (axonal transport of the protein synaptophysin and the neurotoxin tetanus toxin) and particles of unknown movement behavior (transport velocity of synaptic superpool vesicles).

Materials and methods

Cell culture and transfection

Hippocampal neuronal cultures were prepared from 1- to 3-day-old Wistar rats (Charles River, Portage, MI) as described (Welzel et al. 2010). Newborn rats were killed by decapitation in accordance with the guidelines of the State of Bavaria. Hippocampi were removed from the brain and transferred into ice-cold Hank's salt solution, and the dentate gyrus was cut away. After digestion with trypsin (5 mg ml^{-1}), cells were triturated mechanically and plated in MEM medium, supplemented with 10% fetal calf serum and 2% B27 Supplement (all from Invitrogen, Taufkirchen). If required, neurons were transfected with synaptophysin-mRFP under control of a synapsin promoter on DIV3 with a modified calcium phosphate method as described (Threadgill et al. 1997; Welzel et al. 2010). Experiments were performed between 10 and 12 days for

synaptophysin experiments, on day 33 for tetanus toxin experiments and on day 23 for FM 1-43 experiments in vitro, respectively.

Imaging

Experiments were conducted at room temperature on a Nikon TI-Eclipse inverted microscope equipped with a 60×, 1.2 NA water immersion objective and Perfect Focus System^{TM}. Fluorescent dyes were excited by a Nikon Intensilight C-HGFI through excitation filters centered at 482 and 561 nm using dichroic longpass mirrors (cutoff wavelength 500 and 570 nm), respectively. The emitted light passed emission band-pass filters ranging from 500 to 550 nm and 570–640 nm (Semrock, Rochester, NY), respectively, and was projected onto a cooled EM-CCD camera (iXon^{EM} DU-885 and iXon^{EM} DU-897, Andor). Cover slips were placed into a perfusion chamber (volume = 500 µl) containing extracellular medium containing (in mM): 144 NaCl, 2.5 KCl, 2.5 $CaCl_2$, 2.5 $MgCl_2$, 10 glucose, 10 Hepes, pH 7.5.

In synaptophysin experiments images were recorded with 500-ms exposure time at 0.5-Hz frame rate.

For the tetanus toxin experiments cultured dispersed hippocampal neurons were incubated for 1 h with 6 nM GST-GFP-TTC for internalization of the toxin fragment. Images were recorded with 500-ms exposure time at a frame rate of 0.2 Hz.

In FM 1-43 experiments synaptic boutons were stimulated by electric field stimulation (platinum electrodes, 10-mm spacing, 1-ms pulses of 50 mA and alternating polarity); 10 µM 6-cyano-7-nitroquinoxaline-2,3-dione (CNQX, Tocris Bioscience) and 50 µM D-amino-5-phosphonovaleric acid (D, L-AP5, Tocris Bioscience) were added to prevent recurrent activity.

Recycled synaptic vesicles were labeled with FM 1-43 (Invitrogen, Karlsruhe). To stain the total recycling pool nerve terminals were loaded with 1,200 pulses at 40 Hz (Ryan et al. 1996; Ryan and Smith 1995) using 2.5 µM FM 1-43. Dye was allowed to remain on the cells for 60 s after stimulation was finished to permit complete endocytosis and was subsequently removed by a 7 min wash-out. The loaded boutons were then stimulated with 600 pulses at 30 Hz to evoke exocytosis. To ensure that synaptic vesicles were transported, presynaptic terminals were completely destained by a twofold stimulation with 900 pulses at 30 Hz (Groemer and Klingauf 2007). Images were recorded with 500 ms exposure time at 2-Hz frame rate. The frame rate was 0.25 Hz for the double total destain stimulation regime with 900 pulses.

For all experiments, resulting image stacks were converted into tagged image file format (TIFF).

Simulations

All simulations and analyses were performed using custom-written MATLAB (The MathWorks, Natick, MA) programs. Preliminary and quality tests of the described method for the velocity determination in kymograph images were done using synthetic images. The accuracy of the algorithm is given by its bias (Cheezum et al. 2001). For its correct calculation the precise knowledge of the lines slope and length is indispensable (Sbalzarini and Koumoutsakos 2005), and we hence simulated kymograph images numerically. The point spread function of the microscope was approximated by a Gaussian profile (Sbalzarini and Koumoutsakos 2005), and white Gaussian noise was added to model the background (Stroebel et al. 2010).

In preliminary tests with binary and Gaussian profile kymograph images, we generated 1,000 images of 250 × 250 size containing lines with random constant slopes between −10 and 10 pixel/frame. Lines were allowed to have random start points between pixel 30 and 220. In the benchmark test for the dependence of the velocity determination error on different velocities (Fig. 1), we simulated binary kymograph images of 250 × 250 pixel size, each containing one line with a slope between −15 to 15 pixel/frame and the random starting point between pixel 30 and 220. Each slope was generated 1,000 times. In computer simulations with respect to the signal-to-noise ratio (SNR) dependence (Fig. 2), kymograph images of 250 × 250 size were generated, including the particle point spread function and a variable background. SNR is defined as: $\mathrm{SNR} = \frac{I}{\sigma}$, where I is the intensity of the particle and σ is the standard deviation of the background (Stroebel et al. 2010). The images contained lines with random velocities between −10 and 10 pixel/frame and random start points between pixel 30 and 220. For each SNR, 500 independent measurements were done.

Data analysis

The analysis of the kymograph images was performed according to following scheme (Fig. S1, Fig. S2): In a first step a binary image was created from a real data kymograph image as this is a prerequisite for the later Hough transform (Hough 1962). Thereby, the information loss with respect to the trajectory direction and slope has to be minimized. We resorted to the Canny edge detector (Canny 1986), which enables us to detect the edges of the particle trajectories. Due to the Gaussian shape of the particles the Canny method detected two edges for one particle. Determination of the center between these two edges resulted in a binary image (Fig. 4, Fig. S3). In a second step we performed the Hough transform: $\rho = x\cos(\theta) + y\sin(\theta)$, where x and y are

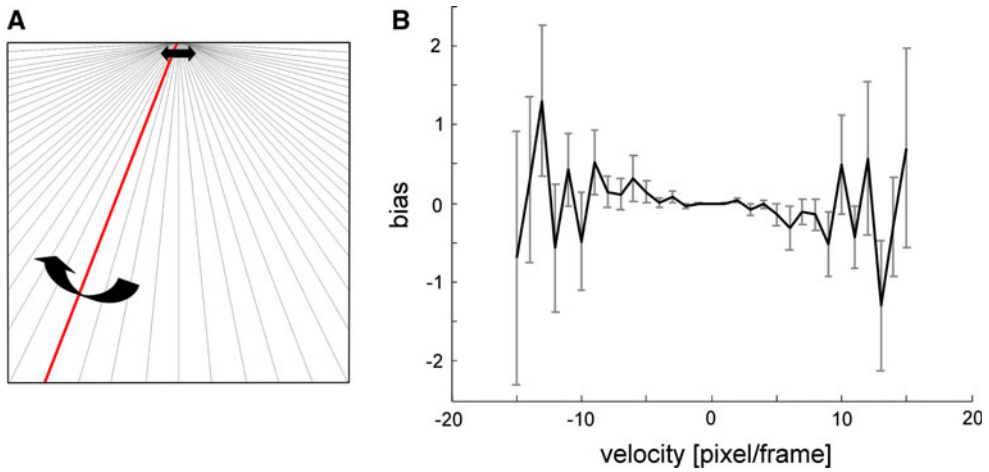

Fig. 1 Dependence of the velocity determination error on the velocity itself. **a** Scheme of simulated binary images used for the test. The starting points (*upper black arrow*) as well as the slopes of the lines (*lower black arrow*) were randomly chosen between preset constraints. **b** Dependence of bias on different velocities. Bias averaged from 1,000 independent simulations. *Error bars* indicate standard deviation. The mean absolute error was 0.51 ± 0.47 pixel/frame for the velocity and 2.06 ± 1.64 pixels for the length of the detected lines

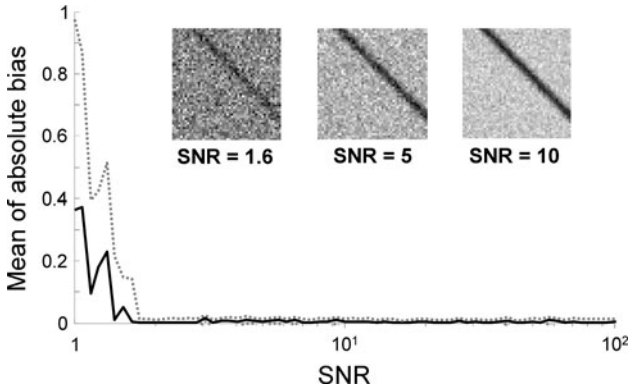

Fig. 2 Benchmark test of velocity determination in kymographs using the Hough transform. The *black line* shows mean of absolute bias versus signal-to-noise ratio (SNR). *Gray lines* indicate corresponding standard deviation. For increasing SNR, the mean and the standard deviation of the absolute bias tend to zero. Each point is averaged from 500 independent simulations. *Insets* show illustrative kymographs for different SNR conditions. The mean of absolute bias is approximately zero for SNR $\geq$ 1.6

the non-zero pixel coordinates of the binary image, ρ is the Euclidian distance (distance origin to foot of perpendicular to the line), and θ is angle between the perpendicular of the line and the x-axis. Thus, the lines are represented in the Hesse normal form instead of using their slope and y-axis intercept. This transform resulted in a parameter space (Fig. 4, Fig. S1). Accumulations in this space represent possible lines in the binary image as they apparently posses the same distance from the origin ρ and the same angle θ. Next we identified those accumulations in the parameter space (Fig. S1). Therefore, we detected local maxima in the parameter space. The maximum number of peaks p to be identified and thus the number of detected lines were restricted by a predefined value. If lines have the same slope and axis intercept, they will be detected without increasing this predefined value of number of peaks. This is because these lines are represented by the same point in the parameter space. For example, a line that is interrupted twice is correctly detected as three single lines with the same slope without increasing the parameter. For each peak p line segments in the binary image were extracted that satisfied the user-defined parameter of minimal line length. The slope, which corresponds to the velocity v, was calculated for the remaining lines by: $v = \tan(-\theta\pi/180)$. All calculated velocities were counted to create a histogram (Fig. 4). In all experiments particles were considered to be moving if their velocitiy was >0.05 μm/s. Consequently particles with velocities <0.05 μm/s were assumed to pause.

Results

Verification and benchmarks

After positive preliminary tests for the proof of principle of the described method (Fig. S1 and "Materials and methods"), we first tested if the Hough transform is able to detect a wide range of possible velocities. This feature might be important especially if, e.g., diverse labeled particles move at different velocities. We simulated synthetic binary kymograph images and determined the error of the velocity determination using the Hough transform. The result of this test is shown in Fig. 1. Here we observed that our method for velocity determination is nearly an unbiased estimator for velocities ranging from −10 to

10 pixel/frame. Velocities that have an absolute value of more than 10 pixel/frame are estimated with less accuracy. Larger errors at larger velocities are due to the tangent function in their calculation (see "Materials and methods") as they exhibit an angle closer to 90°. Nevertheless, their absolute bias is about 1 pixel/frame, and therefore the error is smaller than 10%. For improvement of the velocity range the frame rate has to be increased in order to reduce the pixel-distance traveled by a particle between two frames. Thus, the velocity range depends on the sampling and could be further improved by enlarging our test images, for example. Despite the determination of velocities, the method is able to readout the length of particle trajectories: The mean absolute error for length determination was 2.06 ± 1.64 pixels for all lines with length between 1 pixel and 249 pixels. After verification that our method covers a wide range of possible velocities with high accuracy, we decided to simulate more realistic kymograph images, which include the point spread function of the microscope and noise. As the Hough transform work on binary images (Hough 1962), we first have to convert real data kymograph images. This was achieved using the Canny edge detector (Canny 1986) followed by determination of the center between two detected edges (Fig. S3 and "Materials and methods"). In a next step we compared the results obtained from binary, Gaussian profile and Gaussian profile with noise kymograph images (Fig. S4), where the Gaussian profiles each represented the point spread function of the optical system (Sbalzarini and Koumoutsakos 2005). In all cases the absolute error for the velocity was negligible (binary: 0.06 ± 0.11 pixel/frame; Gaussian profile: 0.08 ± 0.08 pixel/frame and Gaussian profile with noise: 0.07 ± 0.33 pixel/frame; Fig. S4). In contrast the error in the determination of trajectory lengths was higher in kymographs with Gaussian profile compared to binary images (binary: 0.30 ± 3.66 pixel; Gaussian profile: 8.57 ± 2.72 pixel and Gaussian profile with noise: 9.17 ± 2.66 pixel; Fig. S4). This is likely due to border effects at creation of a binary image, where the determination of the center between two detected edges fails as the particle exhibits only one edge at the left and right image border. Therefore, the length of particle trajectories touching the border is underestimated. Last we tested the robustness of the used method due to different SNRs (Fig. 2). For increasing SNR the mean and standard deviation of the absolute bias tend to zero, and thus accuracy of the algorithm is very high for SNR $\geq$ 1.6 (Fig. 2).

Validation via noise replacement

After successful verification and benchmark tests we wanted to know if individual velocities originate from defined particle trajectories in real data. Therefore, we replaced parts of a trajectory with noise (Welzel et al. 2009) and analyzed the kymograph image again (Fig. 3). This enabled us to assign individual velocities in a histogram to its corresponding part of the trajectory (Fig. 3). Together with the benchmark, these test results show that the Hough transform is a suitable and robust method for analyzing kymograph images.

Kymograph image analysis using the Hough transform: case studies

Three applications for the analysis of neuronal cargo transport are considered. Two of them are well characterized for direct comparison purposes with recent studies: (1) axonal transport of the protein synaptophysin (Roy et al. 2007; Welzel et al. 2009) and (2) axonal transport of the

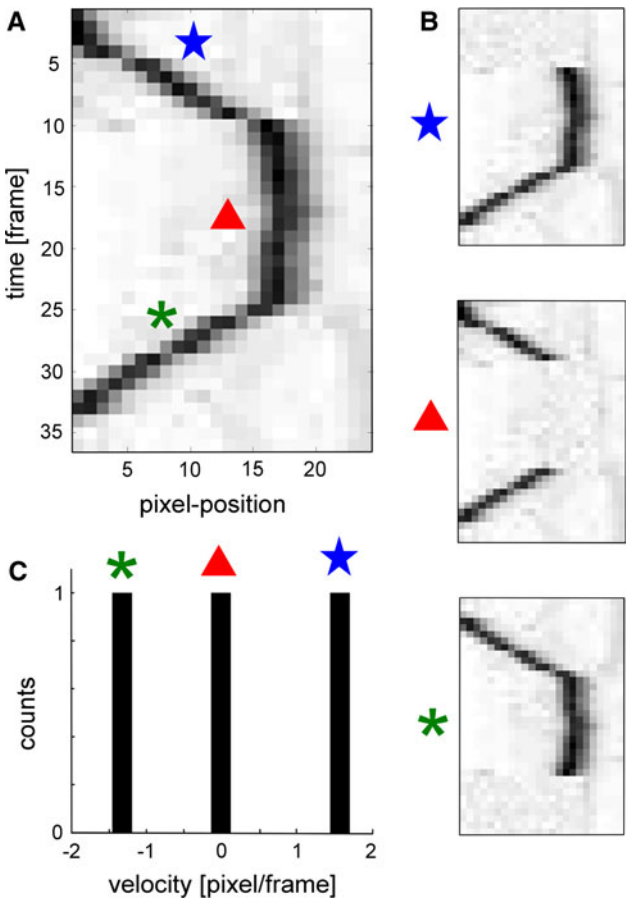

Fig. 3 Assignment of velocities determined by the Hough transform to a particle trajectory via noise replacement. **a** Kymograph obtained from a time-lapse movie (0.5 Hz) of hippocampal neuron, synaptophysin labeled with mRFP. The obvious three different velocities were signed with a *blue star*, a *red triangle* or a *green asterisk*, respectively. **b** Parts of the particle trajectory in the kymograph were replaced with noise to assign to specific velocities in the histogram. **c** Histogram of calculated velocities. Each of the three different velocities was detected as one line and thus resulted in one count for each velocity. Quantification of velocities was omitted for clarity in this case

neurotoxin tetanus toxin (Bohnert and Schiavo 2005; Lalli et al. 2003). Additionally we analyzed the transport velocity of synaptic vesicle sharing between adjacent synapses in hippocampal neurons, which is the focus of our research (Darcy et al. 2006; Staras et al. 2010). Figure 4a shows an example kymograph of synaptophysin labeled with mRFP in a hippocampal axon and the corresponding analysis. The histogram of detected velocities demonstrates that the particles move both anterograde and retrograde with a velocity of about 0.25 μm/s (Fig. 4c). Additionally the pausing time of particles (see "Materials and methods"), which corresponds to the *y*-axis component of the length of the detected lines, is displayed as a histogram (Fig. 4d). The relative pausing frequency was 17.05%. Most particles paused for about 15 s, and about 30% paused double the time in this experiment (Fig. 4d). For verification and consolidation of these results, we increased the number of experiments (Table 1). The average velocity of synaptophysin, which is transported within a wide range of velocities [0.2 μm/s to 3.0 μm/s (Roy et al. 2007)], was 0.80 ± 0.15 μm/s (32 kymographs, 13 experiments) and thus in the range of previous studies (Roy et al. 2007; Welzel et al. 2009). The average pausing time was 39.37 ± 8.83 s and was again in accordance with other studies (Welzel et al. 2009). Furthermore, we analyzed the axonal transport of the neurotoxin tetanus toxin in our primary hippocampal culture (Table 1). This frequently moving toxin (52% moving particles) was found to be transported with an average velocity of around 1 μm/s, as described by other studies (Bohnert and Schiavo 2005; Lalli et al. 2003).

The movement of synaptic vesicles between adjacent synapses was first observed in the frog neuromuscular junction using FM dyes (Betz et al. 1992), and recently it was properly shown that presynaptic terminals are able to share vesicles in hippocampal neurons (Darcy et al. 2006;

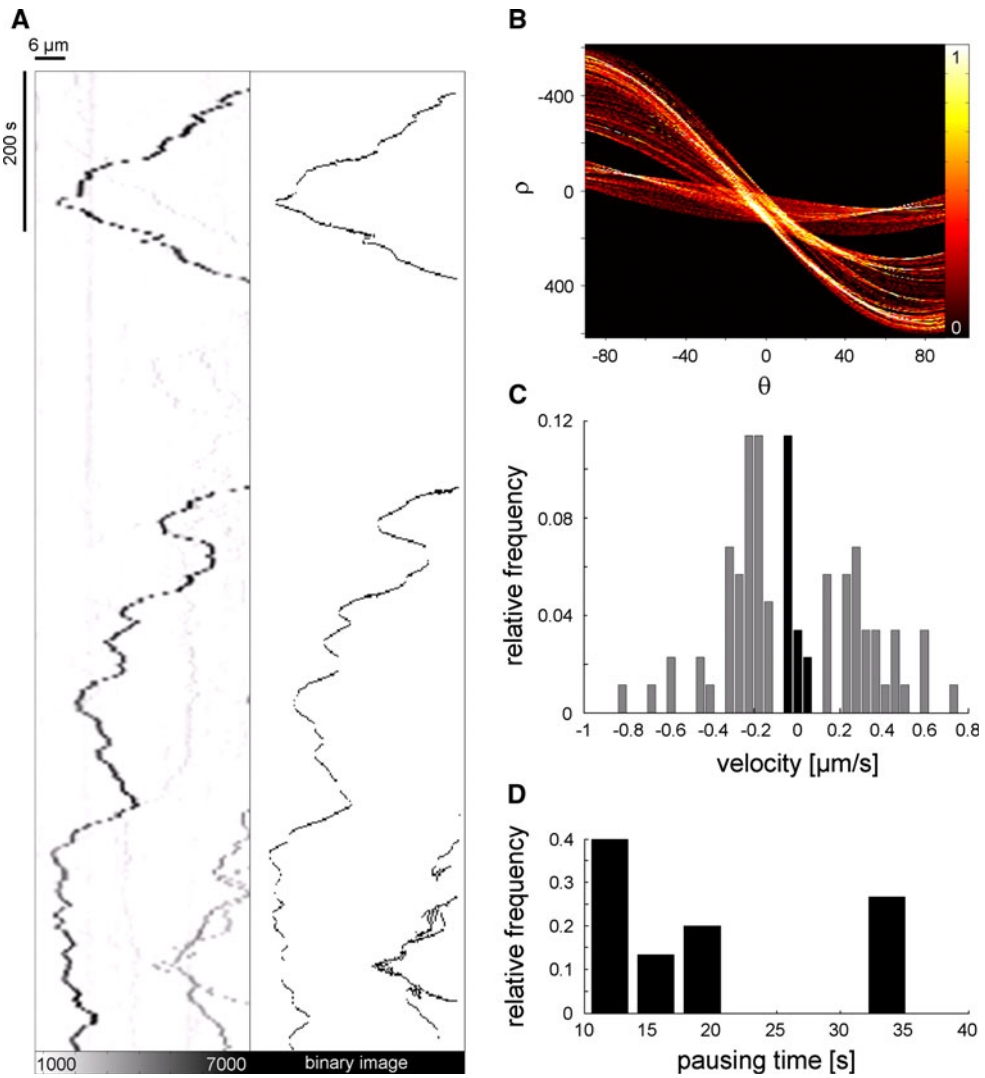

Fig. 4 Example of a kymograph image and its analysis using the Hough transform. **a** *Left* Kymograph obtained from time-lapse movie (0.5 Hz) of hippocampal axon, synaptophysin labeled with mRFP. *Right* Corresponding binary image calculated using Canny edge detector. **b** Parameter space obtained from the binary image using the Hough transform: $\rho = x\cos(\theta) + y\sin(\theta)$. Accumulations in this space represented by local maxima correspond to the angle θ and Euclidean distance ρ of lines in the binary image. The angle can be used to determine the slope and thus velocity v of each detected line: $v = \tan(-\theta\pi/180)$. **c** Histogram of the calculated velocities. The mean of the positive (*right direction*) velocities is 0.30 ± 0.17 μm/s, and the mean of the negative (*left direction*) is −0.23 ± 0.17 μm/s; 39.77% of the detected velocities are positive, and 17.05% are below 0.05 μm/s and thus pausing (*black*). **d** Corresponding histogram of pausing time

Table 1 Quantitative analysis of three different axonal transports: synaptophysin (32 kymographs, 13 experiments), tetanus toxin (7 kymographs, 4 experiments) and "synaptic super pool" (12 kymographs, 5 experiments)

	Fluorescence-label	Example images	Example kymographs	Average velocity (μm/s)	Average pausing time (s)	Estimated % of moving particles
			Position / Time			
Synaptophysin	mRFP	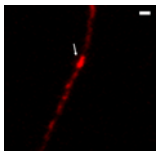	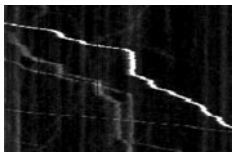	0.80 ± 0.15	39.37 ± 8.83	23.98
TTC	GFP	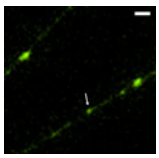	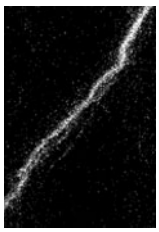	0.97 ± 0.22	25.39 ± 7.23	51.61
Synaptic super pool	FM 1-43	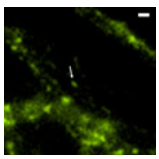	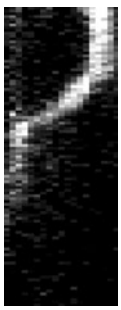	0.11 ± 0.03	–	–

All data are derived from kymograph analysis using the Hough transform. Errors indicate standard error of the mean. Kymograph sizes are as follows: synaptophysin (31.5 μm; 310 s), tetanus toxin (31 μm; 60 s) and "synaptic super pool" (5 μm; 54 s). Scale bars 2 μm

Staras et al. 2010). So far, none of these studies has determined the active transport velocity of this vesicle exchange, while kymographs of this transport have already been shown [see Fig. 4 in (Staras et al. 2010)]. We used our Hough transform method for the determination of these transport velocities. First, we stained the recycling pool of the synapses with FM 1-43 as described (Ryan and Smith 1995). After washing, neurons were stimulated with 600 pulses at 30 Hz to evoke exocytosis. In the following 60 s we made images with a frame rate of 2 Hz to observe vesicle sharing between synapses. To ensure that we looked at transported synaptic vesicles, we completely destained presynaptic terminals by two subsequent stimulation cycles with 900 pulses at 30 Hz (Groemer and Klingauf 2007). Only those shared vesicles were taken into account that reached another synapse and were destained by the double total destain regime. The analysis of this vesicle transport revealed an average velocity of 0.11 ± 0.03 μm/s (Table 1).

Discussion

In this article, we presented a fast and robust method for analyzing kymograph images. We used the Hough transform to extract lines from kymograph images with their slope corresponding to the particle velocity. The Hough transform has successfully been established in the automotive industry (Kamat and Ganesan 1995; Yanamura et al. 2003; Yu and Jain 1997) because of its robustness and fast computational implementation. The advantage for the analysis of axonal transport is the direct control of the results in kymograph images as the output of the Hough transform are extracted lines, which the human observer can directly check for plausibility. These features make the Hough transform a proper technique for analyzing kymograph images and its usage intuitive. However, the Hough transform was made for the detection of straight lines. In a kymograph image, this means particles move at a constant speed. This raises the question whether the method is able

to detect velocities during acceleration and deceleration events of moving particles. As any differentiable function can be approximated by lines according to the Taylor's theorem, the Hough transform can detect bended lines if the sampling rate is chosen adequately. For example, increasing the sampling rate will straighten a parabolic line in a kymograph image. Here the limiting factor will be the SNR as with reduced exposure time of the used camera the SNR will be decreased. The use of kymograph images can increase the SNR because of averaging or taking the maximum of some pixels around the drawn line of interest. This property of kymograph images is an advantage in using higher frame rates.

Besides demonstrating its principle, we tested the efficiency of the used algorithm using simulated data. We found that the described method covers a wide range of velocities in kymograph images (Fig. 1) and can accurately detect velocities at low SNR (Fig. 2). In contrast to other methods (Sbalzarini and Koumoutsakos 2005; Welzel et al. 2009; Zhang et al. 2011), the Hough transform uses the information of the whole image, which results in its robustness with respect to noise (Fig. 2). The lengths of particle trajectories touching the image border are underestimated (see "Results"). In real kymographs of axonal transport, one could reject those trajectories, e.g., by cropping the image, or in large kymograph images with an increasing number of trajectories this border effect is however negligible. We confirmed the applicability of our method to analyzing two well-characterized neuronal cargo transports: the presynaptic protein synaptophysin and the neurotoxin tetanus toxin. Our results were in accordance with those of previous studies (Lalli et al. 2003; Roy et al. 2007). Furthermore, we determined the transport velocity of synaptic vesicles that were shared between synapses (Darcy et al. 2006). The velocity of shared vesicles can be estimated from previous studies as they indirectly also presented information about distance and time of shared vesicles. Ultrastructural analysis revealed that the average separation of synapses was 4.85 μm (Staras et al. 2010), and vesicles were shared over 1–3 adjacent synapses in a 5-min time interval (Staras et al. 2010), resulting in expected velocities ranging from 0.02 to 0.05 μm/s. In the same study a maximal velocity of about 0.02 μm/s could be estimated from fluorescence microscopy data [see Fig. 1G in (Staras et al. 2010)]. Between frog motor nerve terminals the estimated velocity is about 0.01 μm/s [see Fig. 4 in (Betz et al. 1992)]. Our measurement therefore could have resulted in overestimated velocities of transported synaptic vesicles when comparing to these studies. The reason for this discrepancy is that we directly measured the slope and thus the active transport through the axon. In contrast the time used for velocity estimations, which was extracted from previous studies (Betz et al. 1992; Staras et al. 2010), started when vesicles left their original synapse and ended when they had entered their destination synapse. The leaving and entering process and the in and out sorting to vesicle pools were not measured in our direct transport velocity determination and would thus not decrease the average velocity. The here-determined velocity is therefore likely to better represent the transport phase in vesicle sharing.

Automated detection algorithms in basic biological research will hardly outperform an experienced human specialist. However, a method that extracts lines similarly to the human eye enables the human specialist to validate the automated detected results and to eliminate possible error due to operator fatigue. Furthermore, selection criteria could exactly be defined as they are done by the algorithm. Thus, kymograph analysis using the Hough transform allows automated analysis and is therefore capable of high throughput while the operator knows what is happening.

Acknowledgments We thank Katrin Ebert for excellent technical assistance. This work was supported by the Erlanger Leistungsbezogene Anschubfinanzierung und Nachwuchsförderung ELAN Grant Nr. PS-08.09.22.2 and by the Interdisciplinary Center of Clinical Research (IZKF) in Erlangen (Project J5) (both to TWG).

References

Ballard DH (1981) Generalizing the Hough transform to detect arbitrary shapes. Pattern Recogn 13:111–122

Betz WJ, Bewick GS, Ridge RM (1992) Intracellular movements of fluorescently labeled synaptic vesicles in frog motor nerve terminals during nerve stimulation. Neuron 9:805–813

Bilsland LG, Sahai E, Kelly G, Golding M, Greensmith L, Schiavo G (2010) Deficits in axonal transport precede ALS symptoms in vivo. Proc Natl Acad Sci U S A 107:20523–20528

Bohnert S, Schiavo G (2005) Tetanus toxin is transported in a novel neuronal compartment characterized by a specialized pH regulation. J Biol Chem 280:42336–42344

Bonanomi D, Rusconi L, Colombo CA, Benfenati F, Valtorta F (2007) Synaptophysin I selectively specifies the exocytic pathway of synaptobrevin 2/VAMP2. Biochem J 404:525–534

Canny J (1986) A computational approach to edge-detection. IEEE Trans Pattern Anal Mach Intell 8:679–698

Cheezum MK, Walker WF, Guilford WH (2001) Quantitative comparison of algorithms for tracking single fluorescent particles. Biophys J 81:2378–2388

Darcy KJ, Staras K, Collinson LM, Goda Y (2006) Constitutive sharing of recycling synaptic vesicles between presynaptic boutons. Nat Neurosci 9:315–321

DeBolt S, Gutierrez R, Ehrhardt DW, Melo CV, Ross L, Cutler SR, Somerville C, Bonetta D (2007) Morlin, an inhibitor of cortical microtubule dynamics and cellulose synthase movement. Proc Natl Acad Sci USA 104:5854–5859

Deinhardt K, Berninghausen O, Willison HJ, Hopkins CR, Schiavo G (2006) Tetanus toxin is internalized by a sequential clathrin-dependent mechanism initiated within lipid microdomains and independent of epsin1. J Cell Biol 174:459–471

Ekstrom P, Kanje M (1984) Inhibition of fast axonal transport by erythro-9-[3-(2-hydroxynonyl)]adenine. J Neurochem 43:1342–1345

Groemer TW, Klingauf J (2007) Synaptic vesicles recycling spontaneously and during activity belong to the same vesicle pool. Nat Neurosci 10:145–147

Hough PVC (1962) Method and means for recognizing complex patterns. Hough P. V. C., United States

Kamat V, Ganesan S (1995) An efficient implementation of the Hough transform for detecting vehicle license plates using DSP'S real-time technology and applications symposium, 1995. In: Proceedings, pp 58–59

Lalli G, Bohnert S, Deinhardt K, Verastegui C, Schiavo G (2003) The journey of tetanus and botulinum neurotoxins in neurons. Trends Microbiol 11:431–437

Miller KE, Sheetz MP (2004) Axonal mitochondrial transport and potential are correlated. J Cell Sci 117:2791–2804

Miller KE, Sheetz MP (2006) Direct evidence for coherent low velocity axonal transport of mitochondria. J Cell Biol 173:373–381

Morfini GA, Burns M, Binder LI, Kanaan NM, LaPointe N, Bosco DA, Brown RH Jr, Brown H, Tiwari A, Hayward L, Edgar J, Nave KA, Garberrn J, Atagi Y, Song Y, Pigino G, Brady ST (2009) Axonal transport defects in neurodegenerative diseases. J Neurosci 29:12776–12786

Pereira AJ, Maiato H (2010) Improved kymography tools and its applications to mitosis. Methods 51:214–219

Roy S, Zhang B, Lee VM, Trojanowski JQ (2005) Axonal transport defects: a common theme in neurodegenerative diseases. Acta Neuropathol 109:5–13

Roy S, Winton MJ, Black MM, Trojanowski JQ, Lee VM (2007) Rapid and intermittent cotransport of slow component-b proteins. J Neurosci 27:3131–3138

Roze E, Bonnet C, Betuing S, Caboche J (2010) Huntington's disease. Adv Exp Med Biol 685:45–63

Ryan TA, Smith SJ (1995) Vesicle pool mobilization during action potential firing at hippocampal synapses. Neuron 14:983–989

Ryan TA, Li L, Chin LS, Greengard P, Smith SJ (1996) Synaptic vesicle recycling in synapsin I knock-out mice. J Cell Biol 134:1219–1227

Salinas S, Bilsland LG, Schiavo G (2008) Molecular landmarks along the axonal route: axonal transport in health and disease. Curr Opin Cell Biol 20:445–453

Salinas S, Schiavo G, Kremer EJ (2010) A hitchhiker's guide to the nervous system: the complex journey of viruses and toxins. Nat Rev Microbiol 8:645–655

Sbalzarini IF, Koumoutsakos P (2005) Feature point tracking and trajectory analysis for video imaging in cell biology. J Struct Biol 151:182–195

Shakiryanova D, Tully A, Levitan ES (2006) Activity-dependent synaptic capture of transiting peptidergic vesicles. Nat Neurosci 9:896–900

Smal I, Draegestein K, Galjart N, Niessen W, Meijering E (2008) Particle filtering for multiple object tracking in dynamic fluorescence microscopy images: application to microtubule growth analysis. IEEE Trans Med Imaging 27:789–804

Staras K, Branco T, Burden JJ, Pozo K, Darcy K, Marra V, Ratnayaka A, Goda Y (2010) A vesicle superpool spans multiple presynaptic terminals in hippocampal neurons. Neuron 66:37–44

Stroebel A, Welzel O, Kornhuber J, Groemer TW (2010) Background determination-based detection of scattered peaks. Microsc Res Tech 73:1115–1122

Threadgill R, Bobb K, Ghosh A (1997) Regulation of dendritic growth and remodeling by Rho, Rac, and Cdc42. Neuron 19:625–634

Welzel O, Boening D, Stroebel A, Reulbach U, Klingauf J, Kornhuber J, Groemer TW (2009) Determination of axonal transport velocities via image cross- and autocorrelation. Eur Biophys J 38:883–889

Welzel O, Tischbirek CH, Jung J, Kohler EM, Svetlitchny A, Henkel AW, Kornhuber J, Groemer TW (2010) Synapse clusters are preferentially formed by synapses with large recycling pool sizes. PLoS ONE 5:e13514

Yanamura Y, Goto M, Nishiyama D, Soga M, Nakatani H, Saji H (2003) Extraction and tracking of the license plate using Hough transform and voted block matching Intelligent Vehicles Symposium, 2003. In: Proceedings. IEEE, pp 243–246

Yu B, Jain AK (1997) Lane boundary detection using a multiresolution Hough transform image processing, 1997. In: Proceedings, international conference on, vol 2, pp 748–751

Zhang K, Osakada Y, Xie W, Cui B (2011) Automated image analysis for tracking cargo transport in axons. Microsc Res Tech 74:n/a. doi:10.1002/jemt.20934

Zhou HM, Brust-Mascher I, Scholey JM (2001) Direct visualization of the movement of the monomeric axonal transport motor UNC-104 along neuronal processes in living Caenorhabditis elegans. J Neurosci 21:3749–3755